AIAA JOURNAL
Vol. 30, No. 9, September 1992

Asymmetric Turbulent Vortical Flows over Slender Bodies

David Degani*
Technion—Israel Institute of Technology, Haifa 32000, Israel
and
Yuval Levy†
NASA Ames Research Center, Moffett Field, California 94035

Time-accurate numerical solutions have been obtained for equations modeling turbulent subsonic flows over a slender ogive-cylinder body of revolution in the high-angle-of-attack regime where a large asymmetry in the mean flow has been observed experimentally. A modified algebraic eddy-viscosity turbulence model was utilized to correctly compute the effects of the asymmetric vortices on the underlying viscous layers. To reproduce any one of the experimentally observed asymmetric flowfields, it was found necessary to add a small geometrical disturbance near the body apex. By determining an appropriate size of the disturbance, it was possible to obtain excellent agreement between numerical results and experimental data for angles of attack of 30 and 40 deg, Reynolds numbers of $Re_D = 3.0 \times 10^6$ and $Re_D = 4.0 \times 10^6$, and several roll angles. When the disturbance was removed, the calculated flowfield returned to its original symmetric shape. These results are similar in behavior to solutions obtained previously for laminar flows. As in the laminar case, results suggest that the origin of the asymmetry is a convective-type instability of an originally symmetric flow.

Introduction

THE flow around slender bodies of revolution at high incidence has been the subject of a large number of experimental and computational studies.[1-15] The simplicity of the geometries of slender bodies of revolution and their similarities to the shapes of aircraft forebodies encouraged scientists to choose them for basic research. However simple its geometry, the flow developed around a body of revolution at high incidence may be highly complex. High-angle-of-attack flow is governed by large regions of three-dimensional separated flow where the boundary layers leave the surface of the body along lines of separation, and roll up on the leeward side of the body to form strong, concentrated vortical flows. For a typical sharp-nosed body, when the angle of attack is kept below $\alpha \approx 20$ deg, the mean flow in its wake remains symmetric. When the angle of attack is increased, the mean flow becomes asymmetric. As a result of the flow asymmetry, significant side forces and yawing moments can be developed.

At still higher angles of attack above $\alpha \approx 30$ deg, the flow becomes highly sensitive to small changes in the geometry of the body or the flow conditions, especially in the vicinity of the tip. Experimental results[1-4,6,7] also show that the asymmetry (and therefore the side force and yawing moment) is highly dependent on the roll angle of the body relative to the oncoming flow (e.g., see Fig. 1 for angle of attack of $\alpha = 40$ deg, results extracted from Refs. 3 and 4). Recent experimental studies[6,7] have indicated that the dependency on the roll angle originates from the sensitivity of high-angle-of-attack flow to small surface imperfections near the body tip; even dust particles accumulating on the tip may alter the results.[6]

Numerical simulations of flow asymmetry were successfully computed in recent years[12-14] for high-incidence subsonic laminar flows. Besides the availability of experimental data, laminar flow conditions were chosen in order to reduce the number of parameters involved in the problem. It was shown numerically[7,12-14] that, when a perturbation fixed in time and space was introduced asymmetrically near the apex of an ogive-cylinder body at angles of attack above 30 deg, the flowfield became highly asymmetric. However, when the perturbation was removed[7,14] the flowfield returned to its original symmetric shape. On this basis it was suggested[12,13] that the asymmetric flow had its origin in a convective instability of the originally symmetric flow. The concept of convective instability was introduced by Briggs[16] and Gaster.[17,18] According to this concept the flow is convectively unstable if the response at an arbitrary point in space to a perturbation grows initially but decays and vanishes with time after the perturbation is removed.

In previous work, Degani and Schiff[9,10] developed a modification to the widely used Baldwin-Lomax eddy-viscosity turbulence model, which rationally accounts for the presence of the leeward-side vortex structure. Results for supersonic high-incidence turbulent flow, obtained using a parabolized Navier-Stokes method[8] and the modified turbulence model, compared favorably with experimental measurements. It was also shown that the use of the modified turbulence model could be extended to obtain accurate computational results for high-angle-of-attack subsonic[11,15] flows without any further modifications. The subsonic cases were computed using a code based on the time-dependent form of the Reynolds-averaged Navier-Stokes equations. The computations indicated that adequate grid resolution was required to resolve the details of both the viscous boundary layer and the off-surface vortical flow.

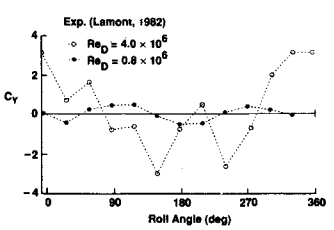

Fig. 1 Side-force coefficient variation with nose roll angle; $M_\infty = 0.28$, $\alpha = 40$ deg (data extracted from Refs. 3 and 4).

Received Sept. 23, 1991; presented as Paper 91-3296 at the AIAA 9th Applied Aerodynamics Conference, Baltimore, MD, Sept. 23-25, 1991; revision received Feb. 27, 1992; accepted for publication Feb. 27, 1992.

*Associate Professor, Faculty of Mechanical Engineering. Associate Fellow AIAA.
†Graduate Student, Stanford University. Member AIAA.

In the computation of the aforementioned turbulent flow cases,[9,10,11,15] it was assumed that the flowfields were symmetric. This assumption can hold as long as the angle of attack is sufficiently low. On the other hand, results of experiments[1-7] show that for higher angles of attack the mean flow behind a slender body is asymmetric, both for laminar and turbulent flow conditions. In the current work we investigate the ability of the modified eddy-viscosity model to simulate asymmetric turbulent subsonic high-incidence flows. We utilize a time-marching thin-layer Navier-Stokes code to compute a series of subsonic turbulent flows over an ogive-cylinder for the following flow conditions: $M_\infty = 0.2$, angle of attack $\alpha = 30$ deg, $Re_D = 3.0 \times 10^6$ and $Re_D = 4.0 \times 10^6$; and $M_\infty = 0.28$, $\alpha = 40$ deg, $Re_D = 3.0 \times 10^6$. It will be demonstrated that, as was shown for laminar high-incidence flows,[12-14] it is necessary to add a space-fixed, time-invariant geometrical disturbance near the tip in order to sustain a perturbation of the convectively unstable symmetric flow that enables the flow to switch to a stable asymmetric form.

Theoretical Background

Governing Equations and Numerical Algorithm

The conservation equations of mass, momentum, and energy can be represented in a flux-vector form that is convenient for numerical simulation as[19]

$$\partial_\tau \hat{Q} + \partial_\xi(\hat{F} + \hat{F}_v) + \partial_\eta(\hat{G} + \hat{G}_v) + \partial_\zeta(\hat{H} + \hat{H}_v) = 0 \qquad (1)$$

where τ is time and the independent spatial variables ξ, η, and ζ are chosen to map a curvilinear body-conforming grid into a uniform computational space. In Eq. (1), $\hat{Q}$ is the vector of dependent flow variables; $\hat{F} = \hat{F}(\hat{Q})$, $\hat{G} = \hat{G}(\hat{Q})$, and $\hat{H} = \hat{H}(\hat{Q})$ are the inviscid flux vectors, and the terms $\hat{F}_v$, $\hat{G}_v$, and $\hat{H}_v$ are fluxes containing the viscous derivatives. A nondimensional form of the equations is used throughout this work.

For body-conforming coordinates and high-Reynolds number flow, if ζ is the coordinate leading away from the surface, the thin-layer approximation can be applied, which yields[20,21]

$$\partial_\tau \hat{Q} + \partial_\xi \hat{F} + \partial_\eta \hat{G} + \partial_\zeta \hat{H} = Re^{-1}\partial_\zeta \hat{S} \qquad (2)$$

where only viscous terms with ζ derivatives are retained. These have been collected into the vector $\hat{S}$ and the nondimensional Reynolds number Re is factored from the viscous flux term.

The implicit scheme employed in this study is the algorithm reported by Steger et al.[22] The algorithm uses flux-vector splitting[23] and upwind spatial differencing for the convection terms in one coordinate direction (nominally streamwise). By using upwind differencing for the convective terms in the streamwise direction and central differencing in the other directions, a two-factor implicit approximately factored algorithm is obtained. It has been shown that this algorithm is unconditionally stable[24] for a representative model wave equation.

In the present computations the flow at the outer boundary of the computational grid was assumed to be the undisturbed freestream. A no-slip condition was applied at the body surface, and a simple zero-axial-gradient extrapolation condition was applied at the downstream end of the computational domain. An implicit periodic continuation condition was imposed at the circumferential edge of the grid.

Turbulence Model

The coefficients of viscosity and thermal conductivity that are used in Eq. (2) are specified from auxiliary relations. For laminar flow, the coefficient of viscosity is obtained using Sutherland's law, and for turbulent flow the coefficient is obtained from the eddy-viscosity turbulence model reported by Degani and Schiff.[9,10] The coefficient of thermal conductivity is obtained once the viscosity coefficient is known by assuming a constant Prandtl number.

Degani and Schiff developed a modification for high-angle-of-attack flows to the well-known Baldwin-Lomax[20] algebraic model (that was developed for two-dimensional boundary-layer flows, and was based on the two-layer model reported by Cebeci et al.[25]). The modification extends the model in a rational manner to permit an accurate determination of the viscous length scale for high-angle-of-attack flows in regions of crossflow separation, where a strong leeward vortical flow structure exists.

As proposed by Baldwin and Lomax,[20] the turbulence model requires the examination of a quantity containing the local fluid vorticity magnitude to determine the length scale, and thus the eddy viscosity coefficient. The modification made by Degani and Schiff[9,10] permits the examination procedure to differentiate between the vorticity within the attached boundary layers and the vorticity on the surfaces of separation, and thus to select a length scale based on the thickness of the attached boundary layers rather than one based on the radial distance between the body surface and the surface of separation.

The modification can be easily extended for the case of an asymmetric crossflow separation. The rationale for the modification can be understood if we examine the flow structure on the leeward side of a body at incidence, shown schematically in a crossflow plane in Fig. 2. One notes that, despite the asymmetry, the topological structure of the flow in a crossflow plane remains the same as that in a corresponding symmetric flow,[9,10,15] so that the previous description of the flow will still hold with some minor modifications. The flow approaching the line of attachment near the windward plane of symmetry turns and flows circumferentially outward and downstream along the body from the windward toward the leeward side under the action of circumferential pressure gradients. Since the main component of the velocity is along the body, a well-defined boundary layer is developed. On the right-hand side, the boundary layer separates from the body at ϕ_{S1}, the primary separation line, and the fluid leaves the body within a shear layer which rolls up to form a primary vortex structure on the leeward side of the body. A similar primary separation occurs on the left-hand side. The primary vortices induce a flow toward the body surface, resulting in a line of attachment somewhere between the lines of primary separation at $\phi = \phi_{A1}$. The induced downflow turns and flows cir-

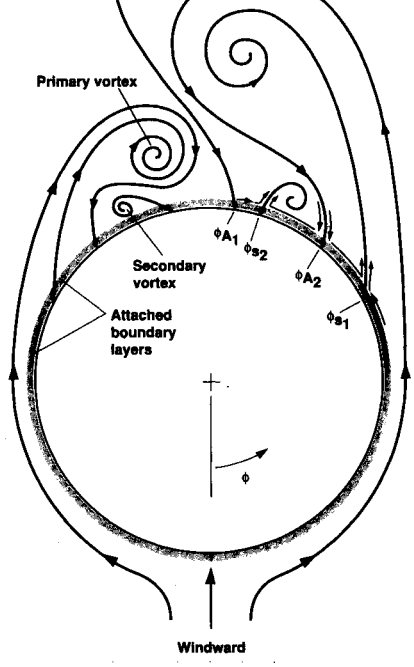

Fig. 2 Schematic of flow structure in crossflow plane.

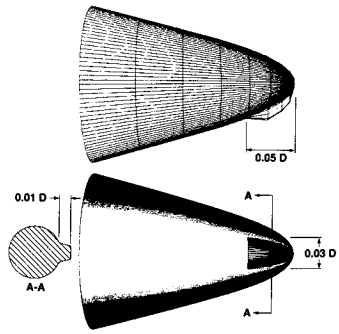

Fig. 3 Detailed geometrical disturbance.

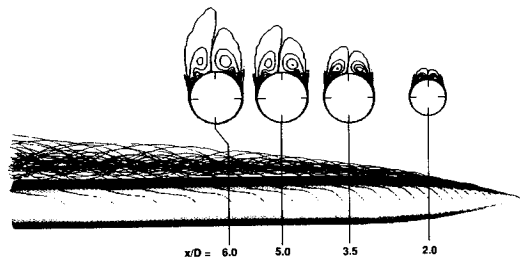

Fig. 4 Computed off-surface streamlines and helicity density contours around an ogive-cylinder body; $M_\infty = 0.2$, $\alpha = 30$ deg, $Re_D = 3.0 \times 10^6$.

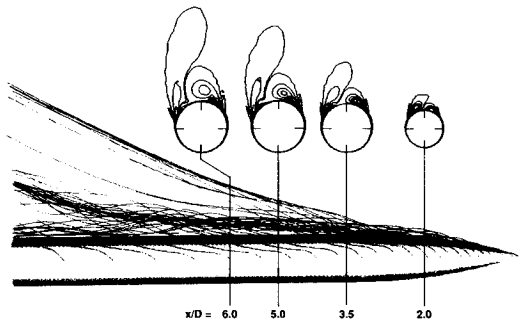

Fig. 5 Computed off-surface streamlines and helicity density contours around an ogive-cylinder body; $M_\infty = 0.2$, $\alpha = 30$ deg, $Re_D = 4.0 \times 10^6$.

cumferentially outward and downstream along the body surface toward the low pressure region generated by the primary vortices. Since the angle of attack of the body is large, and thus the primary vortices are sufficiently strong, this induced boundary-layer flow cannot negotiate the adverse circumferential pressure gradient it encounters beyond the low pressure region of the primary vortex and it separates at ϕ_{S2}, the secondary separation line. Once again, the fluid leaves the body within a shear layer and rolls up behind the body to form the secondary vortex structure. Another line of attachment is located on the body surface between the primary and secondary separation lines, at $\phi = \phi_{A2}$. Similar behavior occurs on the left-hand side. Under certain conditions a tertiary cross-flow separation can occur. The vortex structure itself is essentially inviscid and is dominated by convection of vortical fluid generated within the viscous boundary layer at the body surface rather than by production or dissipation of vorticity along the surfaces of separation. Since the primary direction of the viscous boundary layers is streamwise, it follows that all these layers should be turbulent when the windward-side boundary layer is turbulent.

Further discussion of the effect of the modifications on the computed results are given in the discussion section. Technical details of the model algorithm can be found in Refs. 9 and 10.

Results

A series of subsonic flows was computed about a tangent ogive-cylinder body to illustrate the ability to simulate the turbulent asymmetric flow using the modified turbulence model and to explore the effect of tip disturbances on such flows. In these computations the body had a 3.5-diam tangent ogive forebody with a cylindrical afterbody extending aft of the nose-body junction for 4.0 diameters. This body geometry has been extensively tested by Lamont[4] in the Ames 12-ft pressure wind tunnel, where detailed surface pressure distributions were obtained at Reynolds numbers ranging from $Re_D = 2.0 \times 10^5$ to $Re_D = 4.0 \times 10^6$ and at angles of attack ranging from $\alpha = 20$ to 90 deg.

Computations were carried out to simulate turbulent flow about the tangent ogive-cylinder body at $M_\infty = 0.2$ and angle of attack of $\alpha = 30$ deg and at $M_\infty = 0.28$ and $\alpha = 40$ deg. These conditions were chosen to match those of the experiment.[4] Most of the computations were done using the modified[9,10] turbulence model. All of the turbulence model parameters, including the cutoff distance, were identical to the ones used for the computation of subsonic high-incidence, symmetric flows.[15] The physical grid used for the computations consisted of 120 equispaced circumferential planes extending completely around the body. In each circumferential plane the grid contained 50 radial points between the body surface and the computational outer boundary and 59 axial points between the nose and the rear of the body. The grid was clustered in the radial direction to resolve the viscous layer near the body surface. The nondimensional cylinder diameter was 1.0 and the minimum radial grid spacing at the body surface was 0.00001 to maintain a value of $y^+ < 5$ at the first shell of points above the surface, and to have at least 20 grid points within the viscous layer. Since a zero-gradient extrapolation outflow boundary condition was used, the computed body length was extended 3.0 diameters beyond the physical length of the body to a total of 10.5 diameters to minimize the effect of the outflow boundary.

To simulate a symmetry-breaking imperfection, a geometrical disturbance was added near the body apex as can be seen in Fig. 3. The height of the bump was varied from $0.001D$ to $0.012D$ (~ 0.025–0.25 of the local diameter), where D is the diameter of the cylindrical part of the body (the reader should note that the length of the portion of the body shown in the figure is <2% of the total body length). The numerically simulated disturbance is intended to represent a lump sum of small imperfections of the wind-tunnel model nose. The net effect of such a sum of imperfections causes a different disturbance to the flowfield at each roll angle. The choice of the axial location of the bump was based on previous numerical simulations[14] and experimental results[7] which show higher sensitivity of the flow when the disturbance is placed closer to the apex. The size of the bump was chosen initially according to the degree of asymmetry of the experimental results. With the location fixed, the bump height was varied until the asymmetry achieved in the computation matched the experimental one. Implicit here is the assumption that a disturbance of a particular size at a given circumferential position at the nose will trigger a particular asymmetric flow. Thus a systematic alteration of the size of that disturbance will eventually produce the particular asymmetric flow that was observed in the experiment.

Although the imperfection is simulated by one disturbance only, the size of the bump is of the same order of magnitude as that of the experimental imperfections. A close examination of the tip of an experimental model[6] shows that its natural distortion is of the same order as that of the bump of the current calculation.

A time-accurate solution was computed starting from freestream initial conditions, or from previous calculations. The solution was considered to have converged to a steady state after (L_2NORM) dropped at least three orders of magnitude.

Subsonic Ogive-Cylinder Flow at $\alpha = 30$ deg

The computed off-surface streamlines for $Re_D = 3.0 \times 10^6$ and $\alpha = 30$ deg are presented in Fig. 4. Also shown in Fig. 4 are computed helicity density[26] contours in several crossflow planes.

Helicity density is defined as

$$H_d = V \cdot \omega \tag{3}$$

where V is the velocity and ω is the vorticity. The helicity density has recently been introduced as a tool for graphical representation of three-dimensional flowfields that contain concentrated vortices. The use of this quantity filters out the flowfield regions of low vorticity, as well as regions of high vorticity but low speed, where the angle between the velocity and vorticity vectors is large (such as in the boundary layer). Its use helps to identify and accentuate the concentrated vortices, differentiate between primary and secondary vortices, and mark their separation and reattachment lines. Calculations of helicity density were performed in a manner similar to that of the flowfield calculations by using second-order finite differences in a curvilinear coordinate system. Therefore, these results have the same order of accuracy as those of the flowfield calculations.

Although a small geometrical disturbance was placed near the body apex ($h/D = 0.0025$), only a small asymmetry can be observed, mainly along the aft part of the body. On the other hand, when a larger disturbance was used ($h/D = 0.01$), the flowfield became highly asymmetric, as can be seen from the computed off-surface streamlines and the computed helicity density contours presented in Fig. 5. (Here the Reynolds number is $Re_D = 4.0 \times 10^6$ in order to match a different case of Lamont's experiments.[4])

The differences between the small and large asymmetry can be observed by comparing Figs. 4 and 5, especially by comparing helicity density contours for the two computed cases at the axial location of $x/D = 6.0$. From these figures one can see the large asymmetry that the larger disturbance caused, and the reader should keep in mind that the height of the larger bump is only 1% of the cylinder diameter. Although with monocolor helicity density contours it is impossible to distinguish between positive and negative values, each cross section shows the existence of secondary as well as primary vortices.

The off-surface streamlines in Fig. 4 form two almost symmetric primary vortices that are located very close to the upper surface of the body. On the other hand, the primary vortices in Fig. 5 behave differently; the stronger primary vortex (right-hand side in the cross sections) lies close to the upper surface of the body, whereas the other primary vortex moves upward away from the body. Toward the end of the body the vortices become almost parallel to each other and almost parallel to the freestream (which is a fact known from experimental observation).

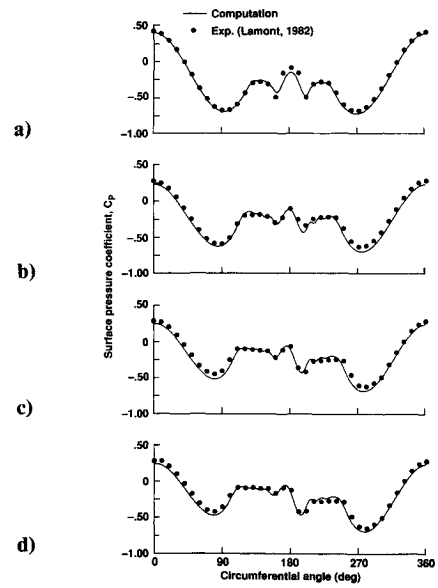

Fig. 6 Computed and measured circumferential surface pressure distributions on different cross sections of the body; $M_\infty = 0.2$, $\alpha = 30$ deg, $Re_D = 3.0 \times 10^6$; a) $x/D = 2.0$; b) $x/D = 3.5$; c) $x/D = 5.0$; d) $x/D = 6.0$.

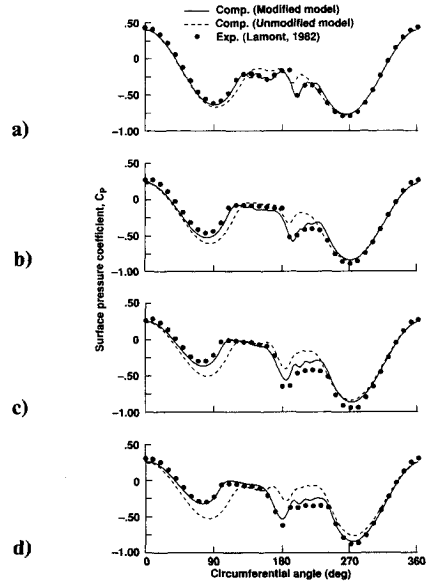

Fig. 7 Computed and measured circumferential surface pressure distributions on different cross sections of the body; $M_\infty = 0.2$, $\alpha = 30$ deg, $Re_D = 4.0 \times 10^6$; a) $x/D = 2.0$; b) $x/D = 3.5$; c) $x/D = 5.0$; d) $x/D = 6.0$.

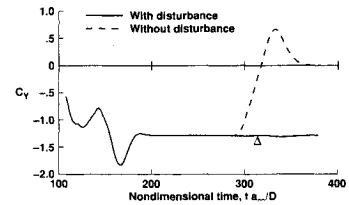

Fig. 8 Side-force coefficient history; $M_\infty = 0.2$, $\alpha = 30$ deg, $Re_D = 4.0 \times 10^6$.

For the small disturbance the computed circumferential surface pressure distributions at several axial locations on the cylindrical portion of the body are shown in Fig. 6, along with Lamont's experimental data.[4] For all axial locations excellent agreement is shown, even for the downstream location of $x/D = 6.0$, where significant asymmetry exists. The results consistently show that the experimental measurements are somewhat higher than the computational results on the windward side of the body. It has been suggested that this disparity might have an experimental origin. The high-angle-of attack flow condition may have directed the windward flow into the pressure taps. Thus, the measured pressure may not have been the surface static pressure, but rather some combination of the surface static and dynamic pressures.

Results obtained with the larger disturbance are compared to data from Lamont's experiment (at a different roll angle) in Fig. 7. The Reynolds number of the computations is $Re_D = 4.0 \times 10^6$ to match the Reynolds number of the experiment. Here, the computed circumferential surface pressure distributions on the cylindrical portion of the body show much larger asymmetry. Again, excellent agreement with the experimental data is obtained. Differences in the flow between this case and the previous one (Fig. 6) are reflected in both the measured and the computed values of the surface pressure

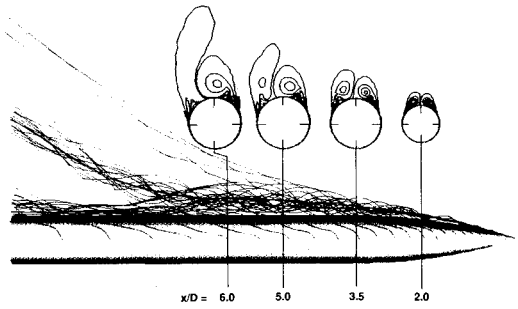

Fig. 9 Computed off-surface streamlines and helicity density contours around an ogive-cylinder body; $M_\infty = 0.2$, $\alpha = 40$ deg, $Re_D = 3.0 \times 10^6$.

coefficients. For the small asymmetry case (Fig. 6), one vortex is only slightly stronger than the other, and the difference between the surface pressure coefficients on opposite sides of the angle-of-attack plane is small. For the large asymmetry case the differences in strength and position between the primary vortices are large, resulting in a large difference in the surface pressure coefficients in the circumferential direction (the most obvious difference is at $x/D = 6.0$). Close examination of Figs. 6 and 7 shows that the flows are asymmetric on the windward side of the body ($\phi \approx 0$ and 360 deg), as well as on the leeward side.

Also noticeable in both cases is the ability of the numerical solution to reproduce a significant feature of experimental data, namely, the existence and behavior of a sharp local minimum in surface pressure coefficient C_P, which is caused by the presence of the secondary vortex at $\phi \approx 180$ deg. The experimental data show that, as the circumferential position of the secondary vortex changes on its path down the length of the body, the position of the local minimum in C_P changes with it, and both of these evolutions are captured faithfully by the numerical results (Figs. 6 and 7).

On the other hand, a solution obtained for the same flow conditions using the unmodified Baldwin-Lomax turbulence model (Fig. 7) is far from satisfactory. Use of the unmodified model in the vortex region yields values of the eddy-viscosity coefficient that are too large, especially in the vicinity of the farthest primary vortex. As a result this vortex becomes weaker and the amount of asymmetry decreases substantially, as can be seen from the dashed line in Fig. 7. It also can be noted that with use of the unmodified model the effect of the secondary vortex; i.e., the sharp local minimum in C_P at $\phi \approx 180$ deg has almost completely vanished.

For laminar flows,[7,14] removal of the disturbance after a steady asymmetric flow had been attained resulted in a decay of the asymmetry and return of the flow to a symmetric state. By the following procedure it was confirmed that the results of computations for turbulent flows behave in the same way. Starting from the converged steady asymmetric case of $\alpha = 30$ deg and $Re_D = 4.0 \times 10^6$, at a certain instant ($ta_\infty/D = 284$) the disturbance was removed and the computation continued to obtain the new steady-state solution. The side-force-coefficient history of this case is presented in Fig. 8. With increasing time, the side-force coefficient converges toward zero and the flowfield simultaneously becomes almost perfectly symmetric.

In contrast to the laminar flow calculations[12-14] and experiment,[5] which show the existence of a high-frequency unsteadiness of the shear layer, the turbulent cases presented in this paper show no significant evidence of such unsteadiness.

From experiments,[1-5,7] we know that the variation of the side-force coefficient C_Y with roll angle position of the nose has an upper bound. This implies that beyond a certain disturbance size the computed side force of the numerical simulation should be bounded also. To confirm this, the bump height was increased from $0.01D$ to $0.012D$. The initial condition was a converged solution with the previous bump height. The results are shown in Fig. 8. The solid line is the side-force coefficient time history. The instant when the bump height was changed ($ta_\infty/D = 315$) is marked by a triangle. After a small oscillation, the side force converged to the same value that was obtained for the $0.01D$ bump. This trend is consistent with the experimental observations.

Subsonic Ogive-Cylinder Flow at $\alpha = 40$ deg

Computed off-surface streamlines and helicity density contours in several crossflow planes are presented in Fig. 9. The flow conditions for this case were $\alpha = 40$ deg, $M_\infty = 0.28$, and $Re_D = 3.0 \times 10^6$. Although the flow asymmetry is relatively large, only a small disturbance ($h/D = 0.0014$) was required to produce an asymmetry that is similar to that of the experiment.[4] Figure 10 shows the computed circumferential surface pressure coefficient distributions at several axial locations together with the experimental results. As was shown for the case of $\alpha = 30$ deg, excellent agreement is obtained for all axial locations. The close agreement between the computed and the experimental surface pressure coefficients in the vicinity of the stronger secondary vortex (the sharp local minimum in C_P at $\phi \approx 180$ deg in Fig. 10) should be noted again. As in the case at $\alpha = 30$ deg, use of the unmodified turbulence model would have washed out any effect of the secondary vortex.

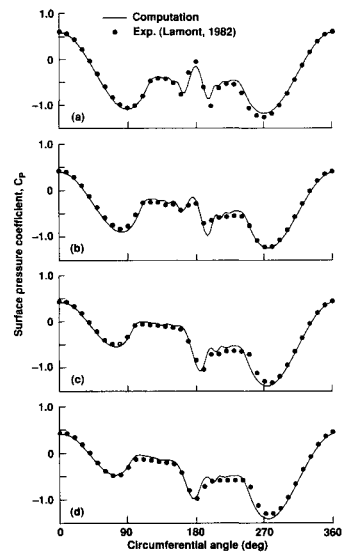

Fig. 10 Computed and measured circumferential surface pressure distributions on different cross sections of the body; $M_\infty = 0.2$, $\alpha = 40$ deg, $Re_D = 3.0 \times 10^6$; a) $x/D = 2.0$; b) $x/D = 3.5$; c) $x/D = 5.0$; d) $x/D = 6.0$.

Fig. 11 Helicity density contours in the cross section at $x/D = 6.0$; $M_\infty = 0.2$, $\alpha = 30$ deg, $Re_D = 4.0 \times 10^6$.

Discussion

To understand why the modified turbulence model gives better results in comparison to the unchanged model (which was developed for two-dimensional boundary-layer flows), one can examine the flow structure at a typical cross section of the flowfield. Figure 11 is a magnification of the helicity density contours at $x/D = 6.0$ of Fig. 5, for the solution obtained at angle of attack of 30 deg with the larger asymmetry (Figs. 5, 7, and 8). The two primary vortices and the secondary ones can be seen very clearly and obviously the flow structure on the leeward side differs from the smooth, attached flow of the windward side. As discussed in the Turbulence Model paragraph of the Theoretical Background section and in Refs. 9 and 10, the outer layer eddy viscosity coefficient is

$$(\mu_t)_{\text{outer}} = KC_{cp}\rho F_{\text{wake}} F_{\text{Kleb}}(h) \tag{4}$$

where K and C_{cp} are constants, ρ is the mass density, F_{Kleb} is the Klebanoff intermittency factor, and

$$F_{\text{wake}} = h_{\max} F_{\max} \tag{5}$$

$F_{\max}$ is the maximum value of $F(h)$:

$$F(h) = |\omega| h[1 - e^{-(h^+/A^+)}] \tag{6}$$

where h is the radial coordinate measured from the body surface, $h_{\max}$ is h where $F_{\max}$ is obtained, and A^+ is a constant. The quantity h^+ is the normal law-of-the-wall coordinate and is defined as

$$h^+ = \frac{\sqrt{\rho_w \tau_w}}{\mu_w} h \tag{7}$$

where ρ_w is the mass density at the wall, τ_w is the wall shear stress, and μ_w is the viscosity at the wall. Several profiles of F, taken along the rays indicated in Fig. 11, are presented in Fig. 12 as functions of h/D. It should be noted that the h/D axis has a logarithmic scale, which means that the actual length for each point is larger than its appearance in the figure. The profile for $\phi = 0$ deg (windward ray) has only one maximum, and the unmodified and the modified models give identical results. This profile is typical for attached boundary layers; therefore, it is easy to determine the value of F_{wake} and from it the value of the eddy-viscosity coefficient.

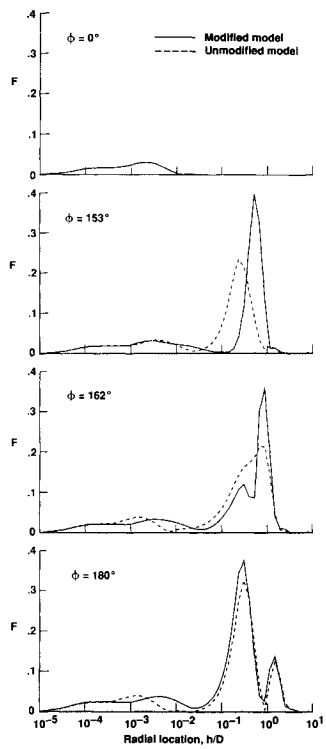

Fig. 12 The F's as functions of radial distance above the body surface along the rays shown in Fig. 11; $M_\infty = 0.2$, $\alpha = 30$ deg, $Re_D = 4.0 \times 10^6$.

On the other hand, on the lee side of the body the profiles of F show more than one peak due to the presence of the vortices, as can be seen from Fig. 12 for circumferential angles of $\phi = 153$, 162, and 180 deg. Obviously, using the second or the third peak to compute the eddy-viscosity coefficient for the underlying boundary layer will result in too large a value. Therefore, in the case of the modified model the search for a maximum of F stops after the first peak. On the other hand, in the case of the unmodified model computation, the additional viscosity washes out the details of the vortex structure; therefore, a large change in the shape of the profiles of F can be seen.

In all cases presented in this study it was found necessary to add a small geometrical disturbance to the body, as depicted in Fig. 3, in order to sustain the convectively stable asymmetric mode. The shape and the circumferential location of the disturbance were the same for all three cases, and the height of the disturbance was the only parameter that was changed to capture the desired asymmetry. The experimental data available to us for $\alpha = 30$ deg were the two cases presented, whereas for $\alpha = 40$ deg the available experimental data included 12 different sets, each corresponding to a different roll angle. For each of these cases, the sectional and the total side force and the circumferential surface pressure coefficient distributions for cross sections along the body were different (see Fig. 1). Although all three cases presented here show excellent agreement between the computational and the experimental results, the achievement of good agreement for cases involving other roll angles might require changes in more than one parameter. Such changes might include the axial location of the disturbance, the circumferential location, or even the introduction of one or several additional disturbances. With more than one parameter in play, matching the influence of an actual geometric disturbance will not be a trivial task. This problem will become important if it is desired to *predict* the asymmetric flow around a given body by means of computation. It will be necessary to know the exact geometry of the body, including the shape of minute imperfections at the tip. The computer simulation will then require sufficient grid resolution to achieve as accurate as possible a reproduction of the body geometry. In principle, achieving a perfect match between the numerically simulated body and the wind-tunnel model should allow computational results to match experimental data for every given roll angle.

Summary

Several high-incidence asymmetric turbulent flow cases were computed. It was demonstrated that the modified turbulence model can be utilized to accurately compute the complex flow structure developed around bodies of revolution at high incidence even when vortex asymmetry is present. Excellent agreement between the surface pressure measurements and computational results was demonstrated.

Analogous to the previous laminar flow calculations, it was necessary to sustain the convectively stable asymmetry mode by adding a small geometrical disturbance near the body apex. Removal of the disturbance resulted in a return of the flow to its original convectively unstable symmetric state. For flows at $\alpha = 30$ deg, it was necessary to use a relatively large disturbance in order to match the relatively small experimentally observed asymmetry. For the flow at $\alpha = 40$ deg, although the experimentally measured asymmetry was relatively large, the size of the disturbance required was much smaller compared to the one required at $\alpha = 30$ deg. This trend is consistent with the trend of results obtained for laminar flow. In contrast to

the previous calculations for laminar flow, no evidence of shear layer unsteadiness was found in the present calculations.

Acknowledgment

This work was supported by the NASA Ames Research Center under Grant NCA2-578.

References

[1]Dexter, P. C., and Hunt, B. L., "The Effects of Roll Angle on the Flow over a Slender Body of Revolution at High Angles of Attack," AIAA 19th Aerospace Sciences Meeting, AIAA Paper 81-0358, Jan. 1981.

[2]Hunt, B. L., "Asymmetric Vortex Forces and Wakes on Slender Bodies," AIAA 9th Atmospheric Flight Mechanics Conf., AIAA Paper 82-1336, Aug. 1982.

[3]Lamont, P. J., "Pressures Around an Inclined Ogive-Cylinder with Laminar, Transitional, or Turbulent Separation," *AIAA Journal,* Vol. 20, No. 11, 1982, pp. 1492–1499.

[4]Lamont, P. J., "The Complex Asymmetric Flow Over a 3.5D Ogive Nose and Cylindrical Afterbody at High Angles of Attack," AIAA 20th Aerospace Sciences Meeting, AIAA Paper 82-0053, Jan. 1982.

[5]Degani, D., and Zilliac, G. G., "Experimental Study of the Nonsteady Asymmetric Flow Around an Ogive-Cylinder at Incidence," *AIAA Journal,* Vol. 28, No. 4, 1990, pp. 642–649.

[6]Zilliac, G. G., Degani, D., and Tobak, M., "Asymmetric Vortices on a Slender Body of Revolution," *AIAA Journal,* Vol. 29, No. 5, 1991, pp. 667–675.

[7]Degani, D., and Tobak, M., "Numerical, Experimental, and Theoretical Study of Convective Instability of Flows Over Pointed Bodies at Incidence," AIAA 29th Aerospace Sciences Meeting, AIAA Paper 91-0291, Jan. 1991.

[8]Schiff, L. B., and Steger, J. L., "Numerical Simulation of Steady Supersonic Viscous Flows," *AIAA Journal,* Vol. 18, No. 12, 1980, pp. 1421–1430.

[9]Degani, D., and Schiff, L. B., "Computation of Turbulent Supersonic Flows Around Pointed Bodies Having Crossflow Separation," *Journal of Computational Physics,* Vol. 66, No. 1, 1986, pp. 173–196.

[10]Degani, D., and Schiff, L. B., "Computation of Supersonic Viscous Flows Around Pointed Bodies at Large Incidence," AIAA 21st Aerospace Sciences Meeting, AIAA Paper 83-0034, Jan. 1983.

[11]Schiff, L. B., Degani, D., and Cummings, R. M., "Numerical Simulation of Separated and Vortical Flows on Bodies at Large Angles of Attack," *Numerical and Physical Aspects of Aerodynamic Flows,* Vol. IV, edited by T. Cebeci, Springer-Verlag, Berlin, 1990, pp. 205–222.

[12]Degani, D., "Numerical Investigation of the Origin of Vortex Asymmetry," AIAA 28th Aerospace Sciences Meeting, AIAA Paper 90-0593, Jan. 1990.

[13]Degani, D., "Effect of Geometrical Disturbance on Vortex Asymmetry," *AIAA Journal,* Vol. 29, No. 4, 1991, pp. 560–566.

[14]Degani, D., and Schiff, L. B., "Numerical Simulation of the Effect of Spatial Disturbances on Vortex Asymmetry," *AIAA Journal,* Vol. 29, No. 3, 1991, pp. 344–352.

[15]Degani, D., Schiff, L. B., and Levy, Y., "Numerical Prediction of Subsonic Turbulent Flows Over Slender Bodies at High Incidence," *AIAA Journal,* Vol. 29, No. 12, 1991, pp. 2054–2061.

[16]Briggs, R. J., "Electron-Stream Interaction with Plasmas," Research Monograph 29, MIT Press, Cambridge, MA, 1964.

[17]Gaster, M., "The Role of Spatially Growing Waves in the Theory of Hydrodynamic Stability," *Progress in Aeronautical Sciences,* Vol. 6, edited by D. Kuchemann and L. H. G. Sterne, Pergamon, New York, 1965.

[18]Gaster, M., "Growth of Disturbance in Both Space and Time," *Physics of Fluids,* Vol. 11, No. 4, 1968, pp. 723–727.

[19]Viviand, H., "Conservative Forms of Gas Dynamics Equations," *La Recherche Aerospatiale,* Vol. 1, Jan. 1974, pp. 65–68.

[20]Baldwin, B. S., and Lomax, H., "Thin Layer Approximation and Algebraic Model for Separated Turbulent Flows," AIAA 16th Aerospace Sciences Meeting, AIAA Paper 78-257, Jan. 1978.

[21]Steger, J. L., "Implicit Finite-Difference Simulation of Flow About Arbitrary Two-Dimensional Geometries," *AIAA Journal,* Vol. 16, No. 7, 1978, pp. 679–686.

[22]Steger, J. L., Ying, S. X., and Schiff, L. B., "A Partially Flux-Split Algorithm for Numerical Simulation of Unsteady Viscous Flows," Proceedings of a Workshop on Computational Fluid Dynamics, Univ. of California, Davis, Davis, CA, 1986.

[23]Steger, J. L., and Warming, R. F., "Flux Vector Splitting of the Inviscid Gasdynamic Equations with Applications to Finite-Difference Methods," *Journal of Computational Physics,* Vol. 40, No. 2, 1981, pp. 263–293.

[24]Ying, S. X., "Three-Dimensional Implicit Approximately Factored Schemes for Equations in Gasdynamics," Ph.D. Dissertation, Dept. of Aeronautics and Astronautics, Stanford Univ., Stanford, CA, June 1986.

[25]Cebeci, T., Smith, A. M. O., and Mosinkis, G., "Calculation of Compressible Adiabatic Turbulent Boundary Layers," *AIAA Journal,* Vol. 8, No. 11, 1970, pp. 1974–1982.

[26]Levy, Y., Degani, D., and Seginer, A., "Graphical Visualization of Vortical Flows by Means of Helicity," *AIAA Journal,* Vol. 28, No. 8, 1990, pp. 1347–1352.